

RSC Advances



This is an *Accepted Manuscript*, which has been through the Royal Society of Chemistry peer review process and has been accepted for publication.

Accepted Manuscripts are published online shortly after acceptance, before technical editing, formatting and proof reading. Using this free service, authors can make their results available to the community, in citable form, before we publish the edited article. This *Accepted Manuscript* will be replaced by the edited, formatted and paginated article as soon as this is available.

You can find more information about *Accepted Manuscripts* in the [Information for Authors](#).

Please note that technical editing may introduce minor changes to the text and/or graphics, which may alter content. The journal's standard [Terms & Conditions](#) and the [Ethical guidelines](#) still apply. In no event shall the Royal Society of Chemistry be held responsible for any errors or omissions in this *Accepted Manuscript* or any consequences arising from the use of any information it contains.

Manipulating Carriers' Spin Polarization in Heusler Alloy Mn₂CoAl

Jian Zhou,^a Baisheng Sa,^b Zhimei Sun,^{*ac} Chen Si^{ac} and Rajeev Ahuja^d

^aSchool of Materials Science and Engineering, Beihang University, Beijing 100191, China

^bCollege of Materials Science and Engineering, Fuzhou University, Fuzhou 350100, China

^cCenter for Integrated Computational Materials Engineering, International Research Institute for Multidisciplinary Science, Beihang University, Beijing 100191, China

^dDepartment of Physics and Astronomy, Uppsala University, 75120 Uppsala, Sweden;

*Correspondence should be addressed to Z.M.S: zmsun@buaa.edu.cn

Abstract

We report that complete spin polarization and controllable spin polarization of carriers can be simultaneously realized in Heusler alloy Mn₂CoAl simply by applying external pressures based on first-principles studies. At ambient conditions, Mn₂CoAl is a ferromagnetic spin-gapless semiconductor (SGS) with complete spin polarization. Under hydrostatic pressures up to 40 GPa, Mn₂CoAl undergoes a series of electronic transitions from SGS with spin-up as conducting channel to ferromagnetic semiconductor and then to SGS with spin-down as conducting channel and finally to half metal, during which the magnetic moment remains as 2μ_B. Such rich electronic transitions are attributed to different responses of the spin-up and spin-down electrons under pressures. This work highlights a desirable way to control the carrier's spin polarization and provides a new insight into the electron behavior in Mn₂CoAl related Heusler alloys under pressures.

1. Introduction

Spintronics, utilizing not only the charge of electrons but also their spins,¹ offer the promise of surpassing the limits of conventional electrical charge-based semiconductor devices with advantages of high speed and low power consumption,^{2,3} and hence attract extensive interests from both academical and industrial communities.^{4,5} To achieve the largest efficiency in a spintronic device, the carrier of the most desirable spintronic materials should be 100% spin polarized. In this case, spin-gapless semiconductors (SGS) and half-metals (HM) are considered as the ideal materials for spintronic devices.⁶⁻⁹ In a spin-gapless semiconductor (or a half-metal) one spin channel has a zero-width band gap (or metallic conducting) while the other spin channel is semiconducting.^{6,7} Due to the zero-width band gap in SGS or metallic behavior in HM no threshold energy is needed to excite the carriers from valence states to conduction states, and hence leading to significantly higher carrier mobility as well as more sensitive response to external field than ordinary semiconductors. SGS exhibits inverted band structure and can be 100% spin polarized for both electrons and holes, indicating the potential applications in spin detectors and spin generators, spin photodiodes.^{6,8} While HM can provide completely spin-polarized current, which holds the advantages of applications in low energy consumption and high speed spin filters and spin rectifier.⁹ Therefore, both spin-gapless semiconductors and half-metals are investigated as novel attractive classes of materials for spintronic devices.^{10,11}

On the other hand, the control of carrier's spin polarization, i.e., the ability to

induce transition between spin-up and spin-down states of electron spins, is another key issue in spintronics, which forms the basis for spintronics and related solid-state quantum information technologies.^{12,13} The spin direction can be switched through reversing the spontaneous magnetization by external magnetic field.¹⁴ However, this approach is not practical due to strong magnetic field needed and not feasible at nanoscale.^{15,16} Recently, electric fields were investigated to be another way for manipulating the spins in spintronics,^{17,18} which practically, however, is a great challenge at some conditions due to the long time (in 100 ns) needed for single-spin rotations.¹⁸ Therefore, exploring alternate easy ways to manipulate electron spins is another important topic in spintronics. Overall, it is pivotal for spintronics devices to search for materials with complete spin polarization and tunable carrier's spin polarization via an easy way. We show that such performance can be realized in Mn_2CoAl Heusler alloy by simply applying external pressures on the basis of first-principles studies.

The Heusler alloy Mn_2CoAl , firstly predicted to be a ferromagnetic half-metal,^{19,20} was later on experimentally verified to be a spin-gapless semiconductor.²¹ Mn_2CoAl exhibits a high Curie temperature of 720 K which is suitable for room temperature applications. The complete spin polarization of its SGS character makes Mn_2CoAl a promising candidate for spintronics in general, such as spin injector, spin photodiodes and spin image detectors.^{6,10,21,22} Very recently, it has been reported that the SGS character in Mn_2CoAl was very sensitive to external strains and dopants,²³ indicating that external pressure could be an alternate way to control the carrier's spin

in Mn_2CoAl as pressure may tune the electronic states around the Fermi level.²⁴⁻²⁹ In fact, external pressure has been proved to be a feasible way to adjust the crystallographic structures and electronic structures in many material systems.²⁸⁻³⁰ Here we show that external pressure is a highly desirable way to manipulate the orientation of electron spins in Mn_2CoAl Heusler alloy on the basis of first-principles calculations. Our results demonstrate that Mn_2CoAl can be simply used in a pressure involved field such as pressure induced spin filter.

2. Computational Methods

The present first-principles calculations are based on the density functional theory (DFT) in conjunction with projector augmented wave (PAW) method, as implemented in Vienna *Ab-initio* Simulation Package.³¹ The standard exchange-correlation potentials of generalized gradient approximations (GGA) of Perdew-Burke-Ernzerhof (PBE) were used.^{32,33} The tetrahedron method with Blöchl corrections was employed for cohesive energy calculation. The relaxation convergences for ions and electrons were set to be 1×10^{-7} and 1×10^{-8} eV, respectively. An energy cutoff of 450 eV and Monkhorst-Pack grids of $8 \times 8 \times 8$ for k-points sampling were used. The wavefunctions of some selected band edge states were calculated by the linearized augmented plane-wave method as implemented in the WIEN2K code.^{34, 35}

3. Results and discussions

Mn_2CoAl crystallizes in a non-centrosymmetric cubic structure (space group no.

216, $F\bar{4}3m$, $C1_b$) of the Hg_2CuTi prototype,²¹ where Mn atoms sit at the Wyckoff positions 4a (0, 0, 0) (hereafter referred to as Mn_A) and 4d ($\frac{3}{4}, \frac{3}{4}, \frac{3}{4}$) (hereafter referred to as Mn_D), while Co and Al atoms locate at 4b ($\frac{1}{2}, \frac{1}{2}, \frac{1}{2}$) and 4c ($\frac{1}{4}, \frac{1}{4}, \frac{1}{4}$), respectively. The crystal structure and its first Brillouin zone are illustrated in Fig.

1. Our calculated equilibrium lattice parameter $a = 5.73 \text{ \AA}$ is identical to that given by S. Skaftouros *et al.*³⁶ and is in agreement with the experimental values of $5.798 \sim 5.839 \text{ \AA}$.^{10,21} Furthermore, Mn_2CoAl remains in the Hg_2CuTi structure up to 76.2 GPa of the present investigated pressure range. This is clearly seen in Fig. 2, which shows the phonon dispersion curves of Mn_2CoAl at ambient conditions, under external pressures of 38.0 GPa and 76.2 GPa, respectively. It is obvious that the phonon dispersion curves of Mn_2CoAl under various pressures are identical except for the increased dispersion frequencies with increasing pressures. Meanwhile, no negative frequency exists under pressures, which confirms the dynamical stability of Mn_2CoAl .

The most exciting finding of this work is summarized in Fig. 3(a), which shows the band gap E_g of the two type spin electrons for Mn_2CoAl under hydrostatic pressures up to 76.2 GPa. It is obvious that the two type spin electrons behave differently under pressures. For the spin-up state, the band gap E_g increases from 0 eV to $\sim 0.25 \text{ eV}$, while for the spin-down state, the band gap E_g firstly increases with increasing pressures up to $\sim 8.0 \text{ GPa}$, and then decreases to 0 eV with further increasing the external pressures to 38.0 GPa, above which the spin-down state is metallic. Overall, the effect of external pressures on the electronic structures of Mn_2CoAl can be illustrated by the schematic density of states in Fig. 3(b). As

illustrated from left to right in Fig.3(b), at ambient conditions, the closed band gap in spin-up channel and an open band gap in spin-down channel demonstrates that Mn_2CoAl is a SGS rather than a half-metal, in good agreement with the experimental results.²¹ Under external pressures, Mn_2CoAl changes from SGS_{up} (spin-up as conducting channel) to common semiconductor below 38.0 GPa and then to SGS_{down} (spin-down as conducting channel) at 38.0 GPa and finally to half metal above 38.0 GPa.

Accompanied with this unique electronic transition in Mn_2CoAl under pressures the local magnetic moments on Mn, Co and Al atoms show slight changes as seen in Fig.4, where the total magnetic moment under various pressures is also included. Obviously, Mn_D atom carries the largest positive local magnetic moment of around $2 \mu_B$ and Co atom possesses a positive magnetic moment of around $1 \mu_B$, whereas Mn_A atom carries the negative magnetic moments of around $-1 \mu_B$. The Al atom is nearly unpolarized. Our results agree well with that of Meinert *et al.*,³⁷ who used the spin polarized relativistic Korringa-Kohn-Rostoker package Munich in their calculations. Even though the absolute values of these local magnetic moments for Mn_A , Mn_D and Co atoms decrease slightly with increasing pressures, the total magnetic moment of Mn_2CoAl remains as $2 \mu_B$ independent of the external pressures, in agreement with the Slater-Pauling rule $M_H = N_V - 24$, where N_V is the number of valence electrons and M_H is magnetic moment per unit cell.^{36,38} Meanwhile, the directions of the magnetic moments are unchanged within the whole investigated pressure range. Our present results clearly show that Mn_2CoAl Heusler alloy is a magnetic spin-gapless

semiconductor at ambient conditions, and an external pressure of around 38 GPa will reverse the carrier's spin polarization but retains this magnetic spin-gapless semiconductor character. On the other hand, a small external pressure, for example (10 GPa as seen in Fig.3a), will transform SGS Mn₂CoAl to a common semiconductor. In a word, the fantastic inversion of complete spin polarization of carriers under pressures will endow Mn₂CoAl Heusler alloy rich performances and multifunctional applications in spintronic devices, such as spin injector, spin filter and spin sensor.

To understand the physical origin of the pressure induced spin transitions in Mn₂CoAl, we show in Fig.5 the spin-resolved band structures under several critical pressures at 0, 8, 38 and 48 GPa, respectively, where the near band edge states around the Fermi level are labeled. At ambient conditions (Fig. 5a), for the spin-up channel, the valence band maximum (VBM) and the conduction band minimum (CBM) touch the Fermi level respectively at Γ point (the Γ_1^- state) and X point (the X_1^+ state) showing a closed band gap, while for the spin-down channel, an indirect energy gap is clearly seen where the VBM and CBM also locate at Γ (the Γ_2^- state) and X (the X_2^+ state) points, respectively. The feature in Fig.5a unambiguously demonstrates that Mn₂CoAl is a spin-gapless semiconductor with spin-up as the conducting channel. By applying external pressures up to 8 GPa, for spin-up channel, the VBM (Γ_1^-) and CBM (X_1^+) move downwards and upwards the Fermi level (Fig.5b), respectively, opening a band gap and hence leading to a semiconducting state. Meanwhile, the energy of the L_1^- state increases and while that of the W_1^+ state remains invariant.

With further increasing pressures, the energy of the L_1^- and X_1^+ states continuously increase and that of the Γ_1^- state decreases, whereas the energy of the W_1^+ state decreases slightly. At 48 GPa, the L_1^- state has higher energy than the Γ_1^- state and hence becomes the VBM, while the X_1^+ state remains as CBM (Fig.5d). Overall, a band gap is opening in spin-up channel that increases with increasing pressures. For the spin-down states under external pressures, as seen from Fig.5a-b, the Γ_2^- state moves slowly towards the Fermi level, and the Γ_2^+ and X_2^+ states move rapidly away from the Fermi level, while the X_4^+ state at just above the CBM moves rapidly downwards the Fermi level. During this period, before the contact of X_2^+ and X_4^+ , the VBM and CBM are still at Γ_2^- and X_2^+ , respectively, which results in the increased band gap as shown in Fig.3a. When the X_2^+ and X_4^+ states reach the same energy level at around 8 GPa, E_g of spin-down state reaches the largest value (Fig.3a). With further increasing pressures at above 8 GPa, the X_4^+ state continues to move towards the Fermi level and then becomes the CBM, thus the band gap gradually decreases. At 38.0 GPa (Fig.5c), both Γ_2^- and X_4^+ states touch the Fermi level and a closed band gap is obtained for spin-down states. It should be noted that at this stage, the Mn_2CoAl alloy transferred from a semiconductor to another SGS with the spin-down as conducting channel. At above 38.0 GPa, the Γ_2^- and the X_4^+ states cross the Fermi level and the spin-down state shows a metallic character. Obviously, the different response of various spin orbitals to pressures around the Fermi level results in the change in carrier's spin polarization and the rich electronic transition as shown in Fig.3. On the other hand, the invariant total magnetic moment under

pressures for Mn₂CoAl can be understood by the band character in Fig.5. The magnetism of Mn₂CoAl is mainly caused by the band inversion of the e_g band,²¹ as seen in Fig.5 the shape of the e_g band is essentially unchanged under pressures, and hence the total magnetism of Mn₂CoAl is kept constant as 2 μ_B . However, distinct different features about the Γ_1^- , X_2^+ and W_1^+ states etc. under pressures are observed in Fig.5, which result in the slight changes in the magnetism moments of Mn_A, Mn_D and Co atoms as shown in Fig.4.

To unravel the responses of the near band edge states to external pressures in Fig. 5, their electronic orbitals and wavefunctions are calculated and analyzed. Firstly, it is worth to mention that in Mn₂CoAl, the closest atomic stacking sequence is Mn_A-Mn_D-Co-Al-Mn_A along the [111] direction, where the atomic distance is 2.48 Å, while the second nearest neighbor is Mn_A-Co (2.86 Å) and Al-Mn_D (2.86 Å) along the [100] direction. Therefore, the interaction between atoms along the [111] direction should be much stronger than that along the [100] direction. Secondly, all the near band states consist of 3d orbitals of Mn_A, Mn_D and Co atoms as analyzed from the projected band structure in Fig.6, that is, the L_1^- state consists of 3d orbitals from Mn_A-Mn_D, Γ_1^- from Mn_A-Co, X_1^+ from Mn_A-Mn_D-Co, W_1^+ from Mn_A-Mn_D, Γ_2^- from Mn_A-Mn_D-Co, X_2^- from Mn_A-Co, X_2^+ from Mn_A-Co, X_4^+ from Mn_D. To reveal the nature of these critical states, their projected wavefunctions are calculated and plotted in Fig.7, where if the sign of the face-to-face wavefunctions from two adjacent atoms are the same (opposite), then bonding (antibonding) orbitals are formed. Keep this in mind, the bond nature of the near band edge orbitals illustrated

in Fig.7 are as following: state L_1^- is antibonding along the [111] direction formed by the nearest Mn_A and Mn_D atoms; Γ_1^- is bonding along the [111] direction by Mn_A and Al atoms; X_1^+ is antibonding along the $\langle 100 \rangle$ direction by the next nearest Mn_A and Co atoms; W_1^+ is nonbonding since there is no interaction between Mn_A , Mn_D and Co atoms; Γ_2^- is antibonding along the [111] direction by Mn_A - Mn_D -Co atoms; X_2^- is antibonding along the $\langle 100 \rangle$ direction by the next nearest Mn_A and Co atoms; X_2^+ is antibonding along [001] and [100] while bonding along [001] by Mn_A and Co atoms which overall has an antibonding character; X_4^+ is bonding along [100] by Mn_D atoms. Combined with Fig.5, it obvious that under external pressures the antibonding states of L_1^- , X_1^+ , Γ_2^- , X_2^- and X_2^+ move towards higher energy level and the bonding states of Γ_1^- and X_4^+ move towards lower energy level while the energy change of the nonbonding state W_1^+ is nearly negligible. It is such different response of bonding and antibonding orbitals under external pressures that results in the present found rich electric transitions of Mn_2CoAl . This response of bonding and antibonding orbitals under pressures can be approximately understood by the Heitler-London's exchange-energy rule through the molecular-orbital model.^{39,40} Similar behavior of bonding and antibonding orbitals under external strains has been reported in two-dimensional phosphorene.²⁷

4. Conclusions

In summary, at ambient conditions Heusler alloy Mn_2CoAl is a ferromagnetic spin gapless semiconductor with spin-up electrons as carrier. Under external pressures up to 40 GPa, Mn_2CoAl will undergo a series of electronic transitions from spin

gapless semiconductor (up spins as conducting channel) to common semiconductor and then to spin gapless semiconductor (down spins as conducting channel) and finally to ferromagnetic half metal. Moreover, the total magnetic moment of Mn_2CoAl remains as $2 \mu_B$ in good agreement with the Slater-Pauling rule. Finally, the rich electronic transitions in Mn_2CoAl under pressures are analyzed to be due to different responses of near band edge orbitals. The present results show that the electronic structure of Mn_2CoAl is very sensitive to external pressures and the carrier's spin polarization can be easily manipulated by pressures, which indicates that Mn_2CoAl may be a good spintronics material used in pressure involved fields, such as filters, sensors and switches. Future experimental work is necessary to further understand this fantastic behavior in Mn_2CoAl . Our present work opens a new avenue to control the carrier's spin polarization of spintronics, and contributes not only to the understanding of Mn_2CoAl related Heusler alloys but also other similar spin gapless semiconductors.

Acknowledgements

This work is supported by the National Science Foundation for Distinguished Young Scientists of China (51225205), the National Natural Science Foundation of China (61274005). R. Ahuja thanks to VR, Sweden for financial support.

References

- 1 B.T. Jonker, S.C. Erwin, A. Petrou and A.G. Petukhov, *MRS Bull.*, 2003, **28**, 740-748.
- 2 S.E. Thompson and S. Parthasarathy, *Mater. Today*, 2006, **9**, 20-25.
- 3 C. Felser, G.H. Fecher and B. Balke, *Angew. Chem. Int. Ed.*, 2007, **46**, 668-699.
- 4 A. Fert, *Rev. Mod. Phys.*, 2008, **80**, 1517-1530.
- 5 A. Fert, *Thin Solid Films*, 2008, **517**, 2-5.
- 6 X.L. Wang, *Phys. Rev. Lett.*, 2008, **100**, 156404.
- 7 R.A. de Groot, F.M. Mueller, P.G. van Engen and K.H.J. Buschow, *Phys. Rev. Lett.*, 1983, **50**, 2024-2027.
- 8 C.L. Kane and E.J. Mele, *Phys. Rev. Lett.* 2005, **95**, 146802.
- 9 H. van Leuken and R.A. de Groot, *Phys. Rev. Lett.*, 1995, **74**, 1171.
- 10 X.L. Wang, S.X. Dou and C. Zhang, *NPG Asia Mater.*, 2010, **2**, 31-38.
- 11 M.I. Katsnelson, V. Yu Irkhin, L. Chioncel, A.I. Lichtenstein and R.A. de Groot, *Rev. Mod. Phys.*, 2008, **80**, 315-378.
- 12 S.A. Wolf, D.D. Awschalom, R.A. Buhrman, J.M. Daughton, S. von Molnar, M.L. Roukes, A.Y. Chtchelkanova and D.M. Treger, *Science*, 2001, **294**, 1488-1495.
- 13 D.D. Awschalom, N. Samarth and D. Loss, *Semiconductor Spintronics and Quantum Computation* (Springer-Verlag, Berlin, Germany, 2002).
- 14 C. Poole, *Electron Spin Resonance* (Wiley, New York, 1983), 2nd ed.

- 15 B. Simovič, P. Studerus, S. Gustavsson, R. Leturcq, K. Ensslin, R. Schuhmann, J. Forrer and A. Schweiger, *Rev. Sci. Instrum.*, 2006,**77**, 064702.
- 16 F.H.L. Koppens, C. Buizert, K.J. Tielrooij, I.T. Vink, K.C. Nowack, T. Meunier, L.P. Kouwenhoven and L.M.K. Vandersypen, *Nature*, 2006,**442**, 766-771.
- 17 Y. Kato, R.C. Myers, D.C. Driscoll, A.C. Gossard, J. Levy and D.D. Awschalom, *Science*, 2003,**299**, 1201-1204.
- 18 K.C. Nowack, F.H.L. Koppens, Yu.V. Nazarov and L.M.K. Vandersypen, *Science*, 2007,**318**, 1430-1433.
- 19 N. Xing, H. Li, J. Dong, R. Long and C. Zhang, *Comput. Mater. Sci.*, 2008,**42**,600-605.
- 20 G. D. Liu, X. F. Dai, H. Y. Liu, J. L. Chen, Y. X. Li, G. Xiao and G.H.Wu, *Phys. Rev. B*, 2008,**77**, 014424.
- 21 S. Ouardi, G.H. Fecher, C. Felser and J. Kübler, *Phys. Rev. Lett.*,2013,**110**, 100401.
- 22 S. Chadov, T. Graf, K. Chadova, X.F. Dai, F. Casper, G.H. Fecher and C. Felser, *Phys. Rev. Lett.*, 2011,**107**, 047202.
- 23 I. Galanakis, K. Özdoğan, E. Şaşıoğlu and S. Blügel, *J. Appl. Phys.*, 2014, **115**, 093908.
- 24 B. Sa, J. Zhou, Z. Song, Z. Sun and R. Ahuja, *Phys Rev B*, 2011,**84**, 085130.
- 25 J. L. Zhang, S. J. Zhang, H. M. Weng, W. Zhang, L. X. Yang, Q. Q. Liu, S. M. Feng, X. C. Wang, R. C. Yu, L. Z. Cao, L. Wang, W. G. Yang, H. Z. Liu, W. Y. Zhao, S. C. Zhang, X. Dai, Z. Fang and C. Q. Jin, *Proc. Natl. Acad. Sci. USA*,

- 2011,**108**, 24-28.
- 26 B. Sa, J. Zhou, Z. Sun and R. Ahuja, *EPL*, 2012,**97**, 27003.
- 27 X. Peng, Q. Wei and A. Copple, *Phys Rev B*, 2014,**90**, 085402.
- 28 Z. Sun, J. Zhou, H.K. Mao and R. Ahuja, *Proc. Natl. Acad. Sci. USA*, 2012,**109**, 5948-5952.
- 29 K. Kotmool, K. Thanayut, C. Sudip, A. Jonas, B. Thiti, W. Luo, H.Y. Gou, C.P. Paulo, T.W. Kang, H.K. Mao and R. Ahuja, *Proc. Natl. Acad. Sci. USA*, 2014,**111**, 17050-17053.
- 30 Z. Sun, J. Zhou, Y.C. Pan, Z.T. Song, H.K. Mao and R. Ahuja, *Proc. Natl. Acad. Sci. USA*, 2011,**108**, 10410-10414.
- 31 J. Hafner, *J. Comput. Chem.*, 2008,**29**, 2044-2078.
- 32 J. P. Perdew, K. Burke and Y. Wang, *Phys. Rev. B*, 1996,**54**, 16533.
- 33 J.P. Perdew and Y. Wang, *Phys. Rev. B*, 1992,**45**, 13244.
- 34 D.J. Singh and L. Nordstrom, *Planewaves, pseudopotentials and the LAPW method* (Springer, Berlin, 2006), 2nd ed.
- 35 K. Schwarz, P. Blaha and G. Madsen, *Comput. Phys. Commun.*, 2002,**147**, 71-76.
- 36 S. Skaftouros, K.Özdoğan, E. Şaşioğlu and I. Galanakis, *Phys Rev B*, 2013,**87**, 024420.
- 37 M. Meinert, J.M. Schmalhorst and G. Reiss, *J. Phys.: Condens. Matter.*, 2011, **23**, 116005.
- 38 I. Galanakis, P.H. Dederichs and N. Papanikolaou, *Phys. Rev. B*, 2002, **66**, 174429.

- 39 W. Heitler and F. London, *Zeitschrift für Physik*, 1927,**44**, 455-472.
- 40 R. M. White, *Quantum Theory of Magnetism*. (Springer, New York, 2006), 3rd ed.

Figure legends

Fig. 1 (color online) Crystal structures and Brillouin zone of Mn₂CoAl. (a) The unit cell has four crystal sites as the basis: A (0, 0, 0), C ($\frac{1}{4}, \frac{1}{4}, \frac{1}{4}$), B ($\frac{1}{2}, \frac{1}{2}, \frac{1}{2}$), D ($\frac{3}{4}, \frac{3}{4}, \frac{3}{4}$) in Wyckoff coordinates. Mn (violet) atoms occupy the A and D sites, while Co (yellow) and Al (gray) atoms occupy the B and C sites, respectively. (b) A scheme of the 3D Brillouin zone of the Mn₂CoAl.

Fig. 2 (color online) The calculated phonon dispersion curves for Mn₂CoAl at various pressures of (a) ambient pressure, (b) $P = 38.0$ GPa, (c) $P = 76.2$ GPa.

Fig. 3 (color online) (a) The calculated band gap E_g under various pressures, where $E_g = E_{CBM} - E_{VBM}$, when $E_g = 0$ eV, the CBM touches the VBM; (b). The schematic density of states $n(E)$ as a function of energy E under external pressures, where the occupied states are indicated by filled areas, and the arrows indicate the majority (\uparrow) and minority (\downarrow) states.

Fig. 4 (color online) The calculated total magnetic moments and magnetic moments on individual atoms under pressures.

Fig. 5 (color online) The calculated band structures of Mn₂CoAl for the spin-up and spin-down electrons under various pressures. (a) at ambient conditions, (b) at 8 GPa, (c) at 38.0 GPa, (d) at 48.0 GPa. The Fermi level is indicated by the short dash dot line at 0 eV.

Fig. 6 The calculated energy band characterization plots at ambient condition of Mn_A,

MnD and Co for the spin-up (a, c, e) and spin-down (b, d, f) electrons. The size of the circles is corresponding to the weight factor of the band characterizations. The Fermi level is set at 0 eV.

Fig. 7 (color online) The projected wavefunctions at ambient condition (blue: positive, red: negative) of the band edge states (a) L_1^- , (b) Γ_1^- , (c) X_1^+ , (d) W_1^+ for the spin-up (majority) electrons and (e) Γ_2^- , (f) X_2^- , (g) X_2^+ , (h) X_4^+ for the spin-down (minority) electrons in Mn_2CoAl . Herein, the blue isosurfaces present the positive wavefunctions and the red isosurfaces show negative wavefunctions. The large purple atoms are Mn, the small yellow atoms are Co and the large grey atoms are Al. The ellipses are guide for eyes.

Fig. 1

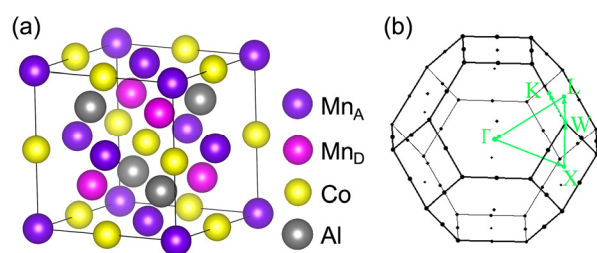


Fig. 2

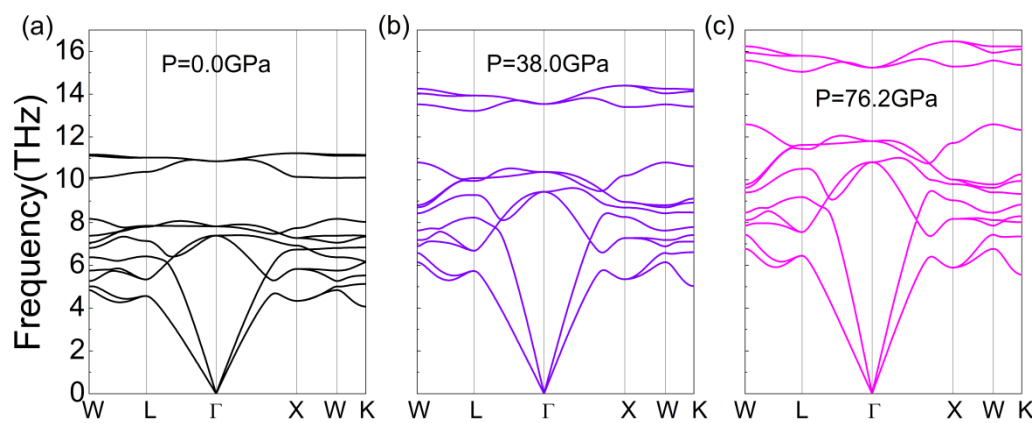


Fig. 3

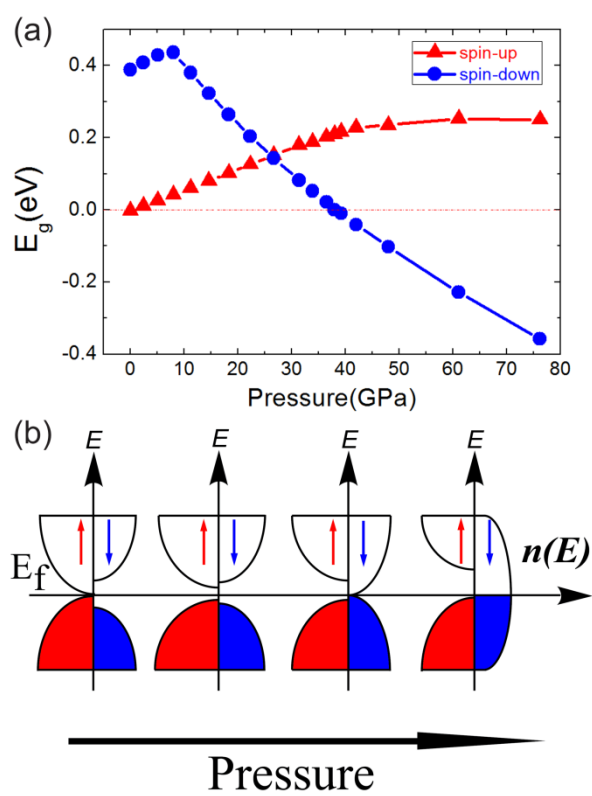


Fig. 4

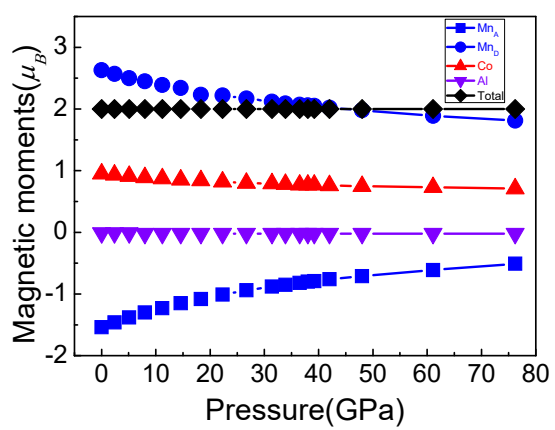


Fig. 5

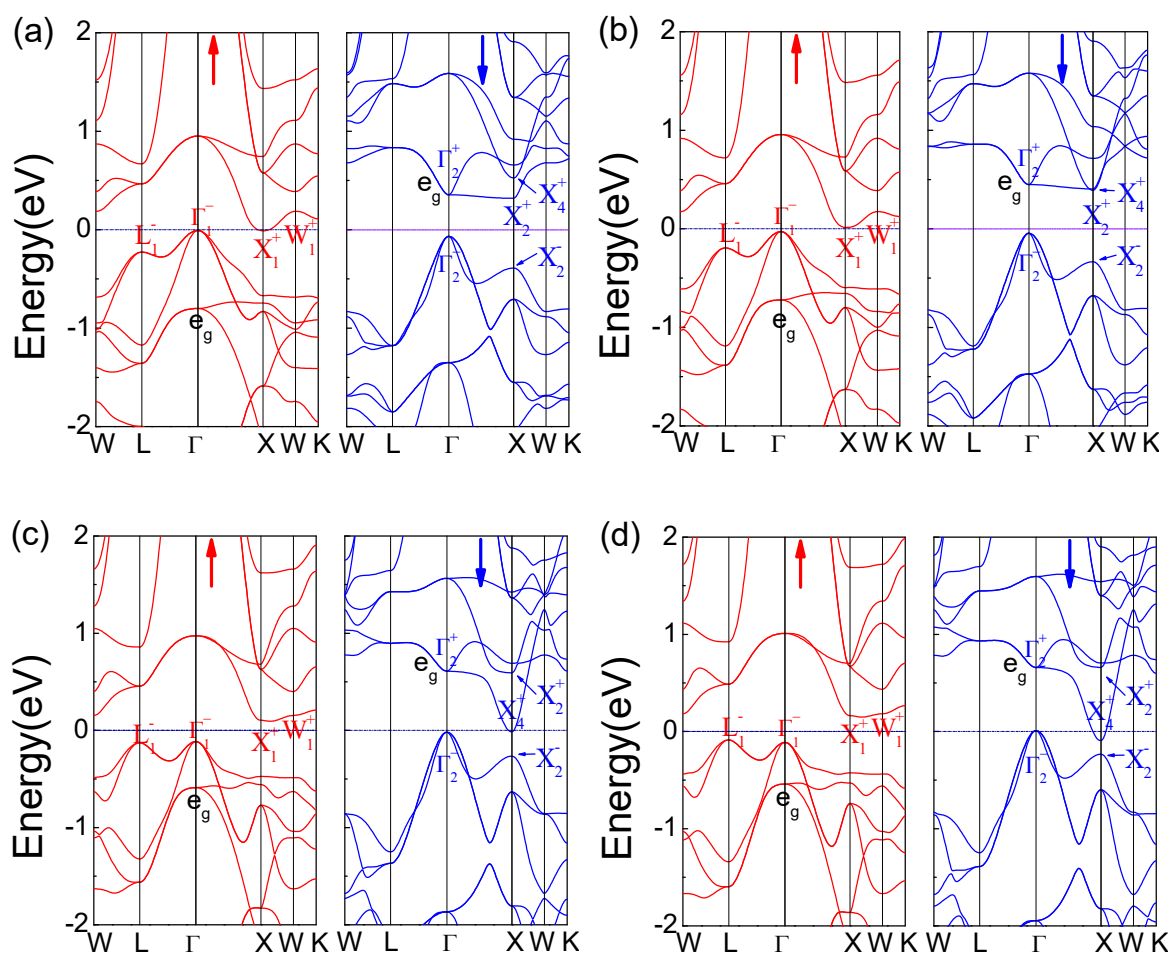


Fig. 6

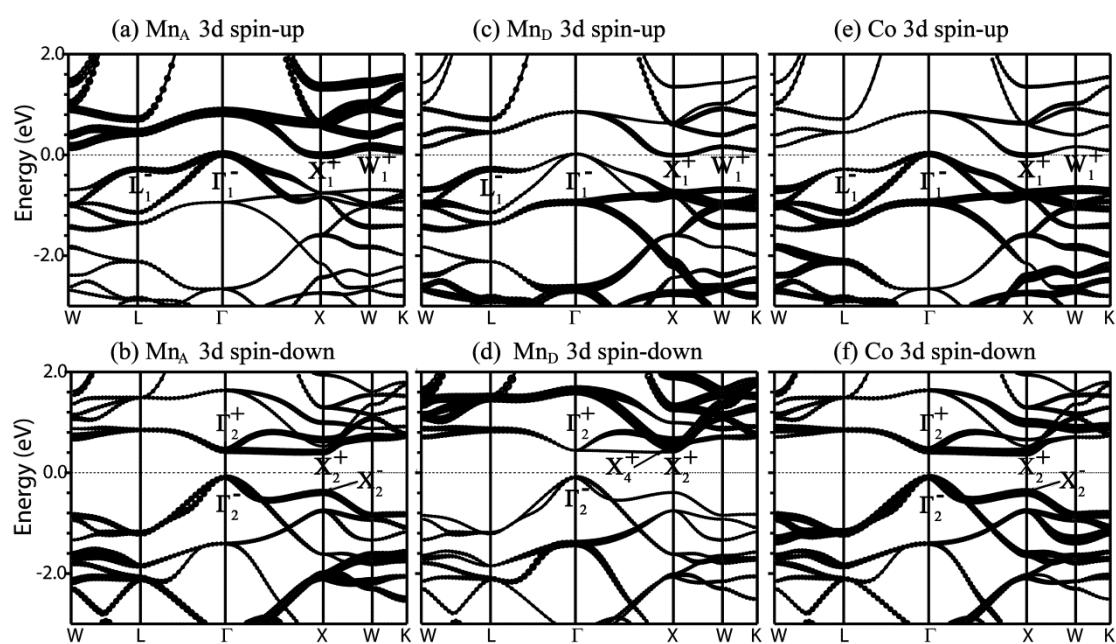


Fig. 7

